Catalysis Science & Technology

ROYAL SOCIETY OF CHEMISTRY

PAPER

View Article Online
View Journal | View Issue

Cite this: *Catal. Sci. Technol.*, 2025, **15**, 5346

The effect of support calcination on carbon supported palladium catalysts for solvent-free benzyl alcohol oxidation

Kai Wang,[a] Samuel Pattisson,*[a] Mark Douthwaite,[a] Matthew B. Conway,[a] Richard J. Lewis,[a] Shengdong Tan,[b] Qian He,[b] David J. Morgan,[a] Stuart H. Taylor *[a] and Graham J. Hutchings *[a]

Received 10th January 2025,
Accepted 12th August 2025

DOI: 10.1039/d5cy00027k

rsc.li/catalysis

Carbon is ubiquitous as a catalyst support used in a wide range of reactions. Various thermal and chemical approaches can tailor the physical properties of the support, such as the surface functionality, to control activity and selectivity. In this study, the effect of pretreatment of the carbon support, *via* calcination, is explored. A series of Pd/C catalysts prepared with increasing calcination temperature, and the final supported catalysts are compared to the untreated sample for their activity in the solvent free aerobic oxidation of benzyl alcohol. The increasing pretreatment temperature coincided with the increased removal of impurities such as sulfur, a higher active metal surface area and an increased acid oxygen functionality. The latter is proposed to dramatically affect metal dispersion resulting in an overall lower intrinsic activity of the catalysts. Interestingly, no effect on selectivity was found when catalysts were studied at iso-conversion. The role of the oxidative treatment was confirmed by comparison to an analogous treatment in nitrogen which had negligible impact on metal dispersion and intrinsic activity compared to the untreated standard material.

Introduction

The selective oxidation of alcohols to their corresponding carbonyl compounds is one of the most studied chemical transformations, both industrially and in academia.[1–4] Among various alcohols, benzyl alcohol has become popular as a model aromatic alcohol to study oxidative upgrading, due to its ease of handling, and the relatively mild reaction conditions employed.[5,6] Additionally, the main product, benzaldehyde, is a non-enolizable aldehyde, which reduces the number of possible by-products and simplifies the study of the catalytic reaction mechanism.[7] Supported Pd catalysts have been widely explored for the efficient catalytic oxidation of benzyl alcohol.[8–15]

One important consideration when preparing efficient heterogeneous catalysts is to select an appropriate support material. The use of carbon, such as activated carbon or carbon black, is common for supported platinum group metals.[16] This class of support offers favourable surface area, chemical stability, recovery of supported noble metals post reaction, and the possibility of tailoring both its textural and surface chemical properties.[17–19] Vulcan XC-72R, a carbon black, has demonstrated particular efficacy as a support for noble metal catalysts in the oxidation of benzyl alcohol and other alcohols and formyls.[20,21] The surface properties of carbon supports can be tuned by applying appropriate thermal or chemical treatments, introducing functional groups, leading to modification of the electronic nature of the surface, acid–base properties, substrate adsorption, surface area, and dispersion of supported metal.[22–26] Calcination (heating in air or oxygen), is a common choice of heat treatment either prior to or following deposition of the active metal onto the support. In the case of carbon, this can aid dispersion of active metal, removal of carbonaceous or other inorganic impurities, and improve activity, selectivity and stability of the final catalysts.[16,27–29]

Herein, a set of supported Pd catalysts were prepared using a sol-immobilization method, where the carbon support (Vulcan XC-72R) was pretreated at varied temperatures in air or N_2 and compared with the untreated carbon. The effect of the thermal pretreatment on the properties of the carbon support and the deposited Pd was studied in detail, using a series of characterization techniques. The catalytic performance of these supported Pd catalysts was subsequently investigated for the solvent-free aerobic oxidation of benzyl alcohol.

[a] *Max Planck–Cardiff Centre on the Fundamentals of Heterogeneous Catalysis FUNCAT, Cardiff Catalysis Institute, School of Chemistry, Cardiff University, Cardiff, CF24 4HQ, UK. E-mail: pattissonsd@cardiff.ac.uk, taylorsh@cardiff.ac.uk, Hutch@cardiff.ac.uk*

[b] *Department of Materials Science and Engineering, National University of Singapore, 9 Engineering Drive 1, Block EA #03-09, Singapore*

Experimental

Materials

Palladium chloride ($PdCl_2$), poly(vinyl alcohol) (PVA, M_w = 9000–10 000, 80% hydrolysed) and sodium borohydride ($NaBH_4$, ≥98%) were purchased from Sigma-Aldrich and used as received. Benzyl alcohol (99%) and *o*-xylene were purchased from Alfa Aesar. Vulcan XC-72 R carbon black was purchased from Cabot Corporation. Deionized water (DI water, 18.2 MΩ) was used for all the solution preparations.

Catalyst preparation

Pd/C catalysts were prepared by a sol-immobilization method, as follows: Aqueous solutions of the metal precursor, $PdCl_2$ solution were added to DI water (140 mL) with vigorous stirring. PVA solution was then added to achieve a PVA/metal weight ratio of 1/1. A freshly prepared $NaBH_4$ solution was added ($NaBH_4$/metal = 4/1, mol/mol), which immediately formed a dark brown colloid. After 30 min of sol generation, the carbon support (0.5 g, Vulcan XC-72R) was added to the colloidal solution with vigorous stirring. The amount of support material required was calculated to have a total final metal loading of 0.7 wt%. After 30 min, the solid catalyst was recovered by filtration and washed repeatedly with DI water (1 L). Finally, the catalysts were dried (110 °C, 16 h) under static air.

The Pd/calcined carbon catalyst was prepared following a similar procedure to that of the Pd/C catalyst. However, the carbon support was pre-treated at 150, 250, or 350 °C under flowing air, or 350 °C in nitrogen, in a tube furnace for 2 h before it was used in catalyst synthesis. The pretreated samples are denoted as Pd/C150, Pd/C250, Pd/C350 and Pd/C350N respectively. Similar nomenclature is used hereafter for the treated and untreated carbon supports (C, C150, C250, C350 and C350N).

Benzyl alcohol oxidation

Benzyl alcohol oxidation was carried out in a 50 mL Colaver reactor. In a typical reaction, the requisite amount of catalyst (72 mg) and pure benzyl alcohol (16 mL) were added into the reactor which was then purged with O_2 five times before the vessel was pressurised to a final gauge pressure of 3 bar, which was maintained throughout the reaction. The mixture was heated to the reaction temperature of 120 °C, unless stated otherwise. The reaction mixture was stirred at 1000 rpm using a magnetic bar inside the reactor. At specified time periods such as 5, 10 or 15 minutes, the stirring was stopped, and the reactor was rapidly cooled in an ice bath. A liquid sample was taken and prepared for analysis. For the analysis of the products, GC (Agilent 7820a, HP-5 column, FID) was employed. The products were identified by comparison with known analytical standards. For the quantification of the amounts of reactants consumed and products generated, an internal calibration method was used employing *o*-xylene as internal standard. Conversion, selectivity and carbon balance were calculated according to the following equations.

$$\text{Conversion (\%)} = \frac{\text{Initial moles of benzyl alcohol} - \text{remaining moles of benzyl alcohol}}{\text{Initial moles of benzyl alcohol}} \times 100$$

$$\text{Selectivity (\%)} = \frac{\text{Moles of product}}{\text{Total moles of all products}} \times 100$$

$$\text{Carbon balance (\%)} = \frac{\text{Remaining moles of carbon}}{\text{Initial moles of carbon}} \times 100$$

To ensure the reproducibility of the results, each test was performed in triplicate.

Catalyst characterization

Transmission electron microscopy (TEM) bright field (BF) images were obtained on a JEOL 2100 (LaB6) instrument fitted with a Gatan Ultrascan 1000xp digital camera operated at 200 kV. Scanning Transmission Electron Microscopy (STEM) high angle annular dark field (HAADF) images were obtained from an aberration corrected JEOL ARM200CF microscope operated at 200 kV. Samples for examination by TEM were prepared by dispersing the dry catalyst powder onto a holey carbon film supported by a 300 mesh copper TEM grid. A particle size distribution (PSD) was calculated by measuring at least 120 particles per sample.

X-ray photoelectron spectroscopy (XPS) analyses were carried out on a Thermo Scientific K-Alpha$^+$ spectrometer utilizing a micro-focused monochromatic Al K_α X-ray source operating at 72 W power (6 mA × 12 kV), all data were recorded in the 400-micron spot mode. Samples were pressed into a copper holder and analyzed at pass energies of 40 and 150 eV for high-resolution and survey scans respectively, this resulted in a C 1s energy of 284.5 eV typical of graphitic carbons. Data analysis was performed in CasaXPS V2.3.26PR1.0N using a Shirley-type background and Scofield cross sections, with an electron energy dependence according to the TTP-2M formula.[30,31] Where required, peak fitting was performed using the LA line shape within CasaXPS using parameters derived from standard materials.

Thermogravimetric analysis (TGA) was performed on a PerkinElmer TGA 4000 apparatus under an atmosphere of flowing air or N_2 (20 mL min^{-1}). The samples were heated from 20 to 900 °C at a heating rate of 10 °C min^{-1} and kept at 900 °C for 5 min. The TGA data were plotted as temperature *versus* weight percentage from which the onset and final decomposition temperatures could be obtained.

The final loadings of samples were analysed, after aqua regia digestion of the catalysts, using an Agilent 7900 ICP-MS instrument, equipped with a micro-mist nebuliser in organic phase mode.

CO chemisorption was performed using a Micromeritics Autochem II 2920 instrument equipped with a thermal conductivity detector. Samples were secured in a u-shaped quartz tube between two pieces of quartz wool and heated in a stream of Ar (50 mL min^{-1}) at a rate of 5 °C min^{-1} to 110 °C for two hours. Subsequently, samples were cooled to 80 °C and treated in a 10% H_2/Ar (50 mL min^{-1}) for four hours. The carrier gas was then switched to Ar (50 mL min^{-1}) whilst maintaining the temperature for 12 hours. After cooling to ambient temperature, the carrier gas was changed to He (50 mL min^{-1}), and samples were heated to 35 °C. Pulses of 1% CO/He were then injected into the carrier gas stream until peak areas remained constant. Reported nanoparticle characteristics were calculated assuming a CO/Pd stoichiometry of 0.5 and equal numbers of the (100), (110), and (111) planes, which have an area of 1.26×10^{19} atoms m^{-2}.[32,33]

N_2 physisorption experiments were carried out at (−196 °C) on a Quantachrome Nova 2200e instrument. All samples (>100 mg) were degassed at 160 °C for 12 h prior to the adsorption experiment. The BET surface area of samples was calculated from the BET equation based on data obtained in the range 0.05–0.2 P/P_0.

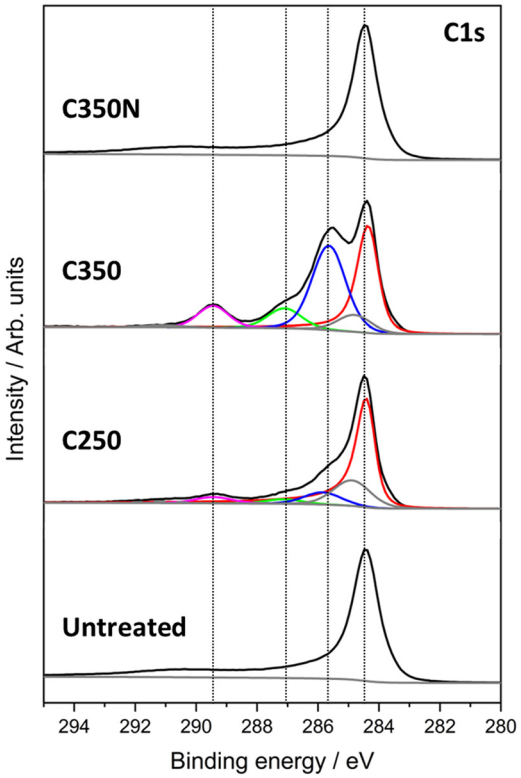

Fig. 1 XPS of C 1s region of untreated carbon, C250, C350, and C350N.

Results and discussion

TGA was first carried out to investigate the thermal stability of the Vulcan XC-72R in air and N_2. The corresponding TGA profiles, which were measured under flowing air are presented in Fig. S1b and c. The carbon exhibited a single oxidation temperature at around 550 °C, suggesting the support should be stable at calcination temperatures below 350 °C. However, upon closer analysis of the TGA profiles, as shown in Fig. S1b, a small decrease in the mass of the sample suggests that a proportion of unknown species were lost between around 250 and 500 °C. The analogous heat treatment under N_2 exhibited a broad mass loss window from *ca.* 250 to 700 °C, resulting in a loss of approximately 0.7 wt% (Fig. S1c). Based on the TGA results, a maximum calcination temperature of 350 °C was chosen, far below that at which carbon loss and major disruption of the support framework would occur. XPS was then performed to investigate the possible changes in surface chemical composition during heat treatment. The XPS survey spectra of various carbon supports (Fig. S2) demonstrated that the major peaks in the spectra belonged to the C 1s, O 1s, and S 2p. The relative atomic concentrations of elements on these carbon surfaces are summarized in Table S1. The low level of sulfur observed in the untreated XC-72R originates from the source material and is common for petroleum-based carbons.[34–36] It is clear that an increase in calcination temperature results in the introduction of a higher amount of surface oxygen and the removal of sulfur, compared to the untreated sample. In contrast, pretreatment with N_2 had a negligible effect on the surface composition of the carbon.

To probe the nature of these functionalities, the C 1s peak was analysed to identify the various individual components (Fig. 1). Table 1 summarizes the corresponding binding energies and relative percentages of each component obtained by curve-fitting analysis.[37–39] The dominant C 1s peak is found at 284.5 eV for all samples, and assigned to graphitic carbon. Given the low concentration of oxygen and sulfur (elemental total less than 1 at%) on both the untreated and C350N samples, fitting of the surface species is subject to high levels of uncertainty. However, analysis of the S 2p and O 1s regions indicate the presence of thiol/disulfide (S $2p_{3/2}$ ~ 164 eV) and predominantly C–O and C–OH functions (O 1s ~ 533 eV) with small contributions from carbonyl containing functions (O 1s ~ 531 eV).[40,41] The low levels of surface functionalisation is supported by analysis of the D-parameter obtained from the first differential of the carbon Auger structure, where both untreated and C350N samples yield a value of 23, characteristic of highly graphitic materials.[39]

Calcination of carbon at 250 and 350 °C, led to significant changes in the carbon surface chemistry. Again, analysis of the D-parameter reveals a significant decrease in the amount of sp^2 carbon atoms (values of 20 and 17 for C250 and C350 carbons respectively) and is also reflected in the C 1s core-level spectra of the calcined materials. The changes in the C 1s spectra are stark and reveal increasing amounts of sp^3 carbon (~285 eV),

Table 1 Results of the peak fittings of XPS C 1s region and relative percentage (at%) of each carbon functionality for the carbon supports

	Binding energy/eV				
	284.5	285.0	286.0	287.0	289.5
Sample	Graphitic carbon (C sp^2)	C–C/C–H	C–O/C–O–C	C═O	COO
C250	64.0	19.0	9.0	3.3	4.7
C350	37.6	7.4	37.5	8.8	8.7

C–O/C–OH (~286 eV), C═O (~287 eV) and COO (~289.5 eV) functionalities, which increase with increasing calcination temperature. The O 1s spectra for both calcined samples reveal similar chemistry, with approximately equal at% signals at 532.5 and 533.9 eV, and are consistent with the assignments made from the C 1s spectra.[39] The observed changes in sp^2/sp^3 content, along with the changes in surface functionality are consistent with what would be expected through oxidation of the carbon surface.[26]

The microstructure of the carbon materials was evaluated by N_2 adsorption (Fig. S3 and Table S2). The untreated carbon has a surface area of 230 $m^2\ g^{-1}$, while the C250 and C350 samples possess a higher surface area of 250 and 260 $m^2\ g^{-1}$, respectively (Table S2). Such an increase in the surface area could be attributed to the partial removal of carbonaceous surface species or contaminants such as sulfur, in addition to the oxidation of the surface, as evidenced by XPS, leading to disruption of the carbon lattice.

A sol-immobilization method was applied to prepare a series of supported Pd catalysts on the above-mentioned carbon supports. In all cases, the actual loading was found to match closely with the nominal value of 0.7 wt% (Table S1), confirmed by ICP-MS. The effect of carbon pretreatment on particle size and distribution was evaluated by TEM, and representative images of the Pd/C and Pd/C350 are displayed in Fig. S4. The average size of Pd nanoparticles was found to be 2.6 ± 0.7 nm and 2.8 ± 0.8 nm in the Pd/C and Pd/C350 catalysts, respectively. Both samples displayed a similar particle size and distribution, and both showed a high degree of uniformity. It is possible that smaller Pd particles and clusters may not be identified due to the limited resolution available *via* the TEM instrument used for this analysis. As such, these samples were further analysed by STEM-HAADF (Fig. 2) and it was found that Pd/C and Pd/C350 catalysts possessed average particle sizes of 2.2 ± 0.8 nm and 1.9 ± 0.7 nm respectively. This result is lower than that observed in TEM, highlighting that the resolution of the instrument can have a significant impact on the accuracy of the acquired data, a point which should be considered when analysing such nanoparticulate catalysts.

To gain a deeper insight on the Pd dispersion in the catalysts, the materials were subsequently probed by CO chemisorption; values for the associated Pd surface areas and dispersion are presented in Table 2. The Pd/C350 exhibited the highest metal dispersion (22%), which is notably higher than that of the Pd/C250 (17%) and Pd/C (11%) analogues. This trend indicates that pretreatment of the carbon support may affect the Pd dispersion. As evidenced by XPS, the calcined carbon has abundant oxygen-containing functionalities on the surface, which could decrease the hydrophobicity of the carbon. As a result, the surface of oxidized carbon becomes more accessible to the Pd nanoparticles during the immobilization in an aqueous solution and thus contributed to the enhanced Pd dispersion.

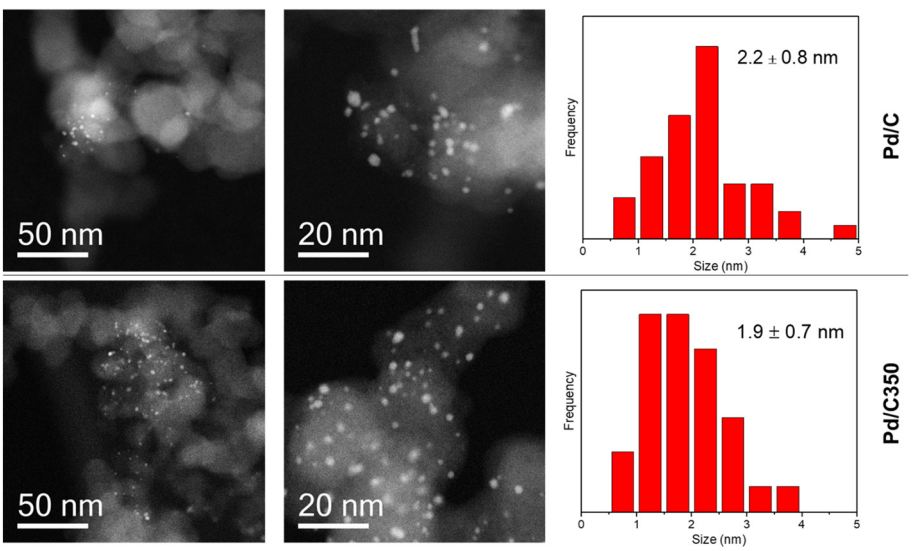

Fig. 2 STEM-HAADF images and corresponding particle size distribution of (top) Pd/C and (bottom) Pd/C350 catalysts.

Table 2 The metal surface area and dispersion of supported Pd catalysts determined by CO chemisorption analysis

Catalyst	Metal surface area/m^2 g_{Pd}^{-1}	Dispersion/%
Pd/C	49	11
Pd/C250	76	17
Pd/C350	97	22
Pd/C350N	54	12

In addition, the oxygen-containing functional groups may serve as anchoring sites for Pd nanoparticles and therefore improve the degree of Pd dispersion. Although this point is not well established in the literature, some researchers have also reported a similar phenomenon.[42] Alternatively, oxidative pretreatment of the support may remove, or induce the mobility of, low molecular weight organic fragments on the surface of the carbon support, which may otherwise result in the poisoning of surface Pd sites. This hypothesis could explain why significant differences in the Pd dispersion is observed, despite the PSDs of the Pd component being comparable. While not confirmed here, other researchers have noted similar observations when synthesising supported metal catalysts with commercial carbon supports.[43,44]

XPS of the corresponding Pd 3d region demonstrates that two sets of peaks were observed for each sample, indicating Pd exists in two different valence states (Fig. S5). The peak at binding energies of approximately 335.9 and 341.2 eV were assigned to Pd $3d_{5/2}$ and Pd $3d_{3/2}$ electrons in the zero-valence, metallic Pd (Pd^0). The other set, at approximately 337.4 and 342.7 eV, was attributed to the presence of the Pd^{2+} state (*i.e.* PdO).[45,46] Table S4 summarizes the calculated percentages of the Pd species in different chemical states and the Pd^{2+}/Pd^0 ratio. For the set of catalysts prepared on pre-calcined carbon, the relative content of the Pd^{2+} species was slightly increased with increasing calcination temperature. It should be noted that during the selective oxidation of alcohols over supported Pd catalysts, Pd sites are believed to undergo reconstruction. In the case of solvent-free benzyl alcohol oxidation, palladium oxide can be reduced to metallic Pd by the adsorbed benzyl alcohol in the initial period of reaction, accompanied by the oxidation of benzyl alcohol to benzyl alkoxide.[11,45]

Table 3 Benzyl alcohol oxidation results over Pd/C, and Pd on variously-treated-carbon supports

		Selectivity/%				
Catalyst	Con./%	TOL	BALD	BB	BEN	CMB/%
Pd/C	32.3	42.8	56.3	0.7	0.2	96.9
Pd/C150	31.9	42.9	56.4	0.6	0.2	96.1
Pd/C250	43.3	43.6	55.9	0.3	0.2	95.7
Pd/C350	51.2	43.5	55.7	0.6	0.2	96.5
Pd/C350N	42.3	42.9	56.3	0.6	0.1	98.7

Reaction conditions: 72 mg of catalyst, 16 mL of benzyl alcohol, 3 bar O_2, reaction temperature 120 °C, stirring rate 1000 rpm, reaction time 15 min. KEY: TOL (toluene); BALD (benzaldehyde); BB (benzyl benzoate); BEN (benzene); CMB (carbon mass balance).

The catalytic oxidation of benzyl alcohol under solvent free conditions was chosen as a model reaction to explore how the differing properties of these materials influences their catalytic performance (Table 3). In all cases, a carbon mass balance (CMB) of between 95 and 99% was observed. The Pd/C catalyst exhibits a 32.3% conversion of benzyl alcohol, and the selectivity to benzaldehyde and toluene is 56.3 and 42.8%, respectively. The Pd/C150 shows comparable activity (31.9%) and selectivity with that of Pd/C. However, when the calcination temperature of carbon was increased to above 150 °C the conversion of Pd/C250 was significantly enhanced to 43.3%, while the Pd/C350 has an even higher conversion of 51.2%. There is no statistical difference in the selectivity of products among these catalysts. The time-dependent catalytic result of benzyl alcohol oxidation further demonstrates that the PdC350 sample has higher activity than the other catalysts over the reaction time (Fig. 3a) however no major differences in selectivity are observed (Fig. 3b). To ensure this was not simply related to the extent of conversion, the reaction times were altered to achieve comparable levels of benzyl alcohol conversion (*ca.* 30%), (Table 4). When compared at iso-conversion, only minor differences in selectivity to toluene and benzaldehyde are observed.

Next, the reaction rates for benzyl alcohol oxidation (TOF_{Tot}) over each of the catalysts were normalised to the number of exposed Pd sites. The normalised intrinsic rate of benzyl alcohol conversion decreases as the proportion of surface oxygen in the catalysts increases (Table 5). Interestingly, the TOF_{tot} for the Pd/C and Pd/C350N are very similar (113 and 117 × 10^{-3} s^{-1}, respectively). Given that these two catalysts possess equally low proportions of surface oxygen, it suggests that the rate of benzyl alcohol conversion is negatively affected by surface oxygen. Given the preceding observations, it was also important to establish whether the reaction selectivity was influenced by the proportion of exposed Pd sites present in each of the catalysts. It is well established that there are two primary pathways which proceed from benzyl alcohol under aerobic conditions: the oxidative dehydrogenation of benzyl alcohol which results in the formation of benzaldehyde, and the disproportionation of benzyl alcohol which produces equimolar quantities of benzaldehyde and toluene (eqn (1) and (2) respectively). In order to quantify the contribution of each pathway on the overall reaction rate and product selectivities, a similar approach was used to our previous work, in which the amount of toluene observed in a reaction is taken as a direct measure of the disproportionation reaction, as under these conditions, toluene is not produced *via* any other route.[47] According to this methodology, the turnover frequency (TOF) was calculated for each pathway; the oxidative dehydrogenation of benzyl alcohol (TOF_O) and the disproportionation reaction (TOF_D), and compared to the total turnover frequency (TOF_{Tot}) (eqn (3)–(5)).

$$PhCH_2OH + \frac{1}{2}O_2 \rightarrow PhCHO + H_2O \quad (1)$$

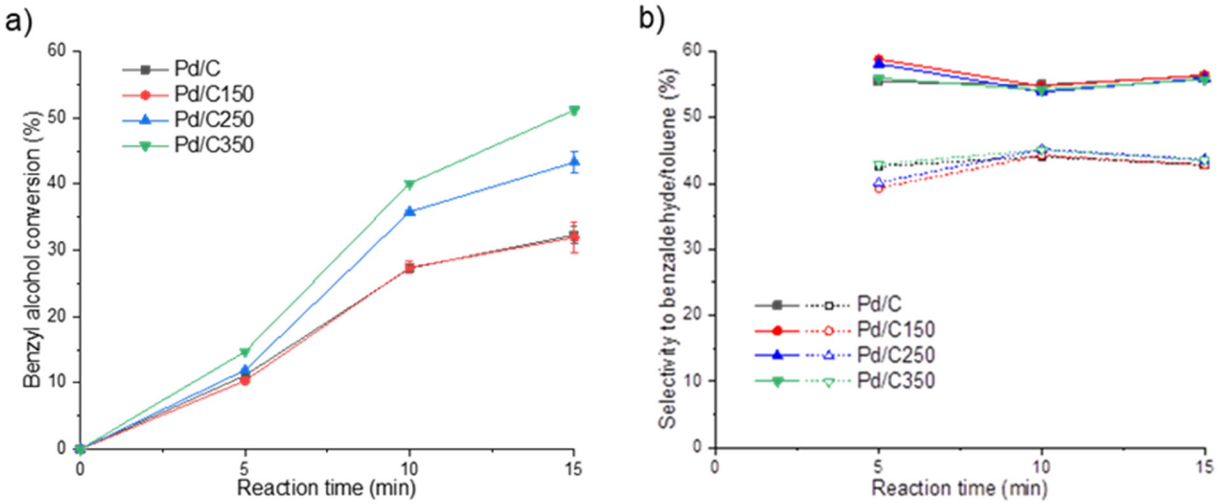

Fig. 3 Catalytic performance for solvent-free benzyl alcohol oxidation. a) Benzyl alcohol conversion and b) product selectivity toward benzaldehyde (solid line) and toluene (dashed line) as a function of time over Pd/C, PdC150, Pd/C250, and Pd/C350. Reaction conditions: 16 mL of benzyl alcohol, 72 mg of catalyst, 3 bar O_2, reaction temperature 120 °C, stirring rate 1000 rpm. Associated error bars were generated by performing each test in triplicate.

$$2PhCH_2OH \rightarrow PhCHO + PhCH_3 + H_2O \quad (2)$$

$$TOF_O = \left(\frac{mol_{PhCHO} - mol_{toluene}}{mol_{metal}}\right)/t \quad (3)$$

$$TOF_D = \left(\frac{mol_{toluene}}{mol_{metal}}\right)/t \quad (4)$$

$$TOF_{Tot} = \left(\frac{converted\ mol_{PhCH_2OH}}{mol_{metal}}\right)/t \quad (5)$$

The calculated TOFs for the disproportionation and oxidative dehydrogenation pathways (TOF_D and TOF_O, respectively), also displayed in Table 5, highlight that the disproportionation reaction is dominant with all the catalysts studied. This is consistent with previous reports for carbon supported Pd catalysts in the solvent free oxidation of benzyl alcohol.[47] Previous work has suggested that selectivity of these competitive pathways can be induced by using supports with considerable acid/base properties[3] but evidently, the oxidation of a carbon surface does not provide sufficient functionalisation to accommodate this chemistry. Here, we see that the relative rates of the disproportionation and oxidative dehydrogenation pathways are proportional, regardless of the support materials surface oxygen content.

While the surface oxygen content of a carbon support has very little impact on the selectivity exhibited by supported Pd nanoparticles in this reaction, it does have a considerable impact on the intrinsic activity of the Pd sites. Calcination of the supports prior to immobilisation of the Pd nanoparticles leads to an increase in the surface oxygen content, reducing the efficacy of the Pd sites towards benzyl alcohol oxidation. Results from CO chemisorption experiments, indicate that the surface oxygen species assist in the dispersion of the Pd, although this was not effectively captured from analogous STEM experiments. Given that this reaction is particularly sensitive to particle size effects,[48] it is likely that the differing activity is attributed to this. Ultimately, this work highlights the importance of using multiple methods for studying particle size effects of heterogeneous catalysts. More development is evidently required in this area, particularly for the study of metals which are not easily probed using rudimentary chemisorption techniques.

Table 4 Comparison of benzyl alcohol oxidation at iso-conversion of *ca.* 30% over Pd/C, Pd/C250, and Pd/C350 catalysts

		Selectivity/%			
Catalyst	Con./%	TOL	BALD	BB	BEN
Pd/C	30.8	45.4	53.8	0.6	0.2
Pd/C250	30.4	45.2	53.9	0.7	0.1
Pd/C350	31.9	45.9	53.2	0.7	0.2

Reaction conditions: 72 mg of catalyst, 16 mL of benzyl alcohol, 3 bar O_2, reaction temperature 120 °C, stirring rate 1000 rpm. KEY: TOL (toluene); BALD (benzaldehyde); BB (benzyl benzoate); BEN (benzene).

Table 5 Calculated turnover frequencies for benzyl alcohol conversion (TOF_{Tot}), the disproportionation reaction (TOF_D) and the oxidative dehydrogenation of benzyl alcohol (TOF_O)

Catalyst	TOF_{Tot} ($\times 10^{-3}$)/s^{-1}	TOF_D ($\times 10^{-3}$)/s^{-1}	TOF_O ($\times 10^{-3}$)/s^{-1}
Pd/C	113	47	15
Pd/C250	99	41	12
Pd/C350	91	38	11
Pd/C350N	117	50	16

Reaction conditions: 72 mg of catalyst, 16 mL of benzyl alcohol, 3 bar O_2, reaction temperature 120 °C, stirring rate 1000 rpm, reaction time 15 min.

Conclusions

Pre-calcination of a carbon support prior to the immobilisation of Pd nanoparticles was determined to have a significant effect on the catalytic performance of the materials in the solvent-free oxidation of benzyl alcohol. This oxidative pre-treatment was determined to remove sulfur impurities from the carbon and introduce an abundance of oxygen containing functional groups. The prepared catalysts were found to contain a higher active metal surface area with increasing calcination temperature, despite appearing to have similar average Pd particle size by STEM analysis. The higher Pd dispersion is found to negatively impact intrinsic activity of the catalysts with no apparent effect on selectivity when measured at iso-conversion. The role of the oxidative treatment was confirmed by analogous heat treatments in nitrogen, which yielded catalysts similar in dispersion and activity to the untreated standard material.

Author contributions

KW, SP, MD, SHT and GJH conceived and conceptualized the project. KW, MBC, ST and DJM conducted the experimental investigation and performed the data analysis. SP, MD, RJL, SHT and GJH provided project supervision. SHT and GJH provided funding acquisition. KW, SP and MD wrote the manuscript. The manuscript was finalized and edited through the contributions of all authors.

Conflicts of interest

The authors declare no conflict of interest.

Data availability

Supplementary information is available: TGA, XPS, nitrogen physisorption, ICP-MS and TEM. See DOI: **https://doi.org/10.1039/D5CY00027K**.

All the data is presented in the paper and in the detailed supplementary data.

Acknowledgements

KW, SP, MD, MBC, RJL, DJM, SHT and GJH would like to thank the Max Planck Centre on the Fundamentals of Heterogeneous Catalysis (FUNCAT) for funding. KW would like to additionally thank the Chinese Scholarship Council for funding. The authors thank the CCI-Electron Microscopy Facility, which has been part-funded by the European Regional Development Fund through the Welsh Government and the Wolfson Foundation. XP spectra were acquired by EPSRC National Facility for Photoelectron Spectroscopy (HarwellXPS), operated by Cardiff University and UCL under contract number PR16195. QH acknowledges the support by National Research Foundation (NRF) Singapore under its NRF Fellowship (NRF-NRFF11-2019-0002).

References

1 D. I. Enache, J. K. Edwards, P. Landon, B. Solsona-Espriu, A. F. Carley, A. A. Herzing, M. Watanabe, C. J. Kiely, D. W. Knight and G. J. Hutchings, *Science*, 2006, **311**, 362–365.
2 I. W. C. E. Arends, Y. X. Li, R. Ausan and R. A. Sheldon, *Tetrahedron*, 2006, **62**, 6659–6665.
3 C. Della Pina, E. Falletta and M. Rossi, *J. Catal.*, 2008, **260**, 384–386.
4 S. Najafishirtari, K. Friedel Ortega, M. Douthwaite, S. Pattisson, G. J. Hutchings, C. J. Bondue, K. Tschulik, D. Waffel, B. Peng, M. Deitermann, G. W. Busser, M. Muhler and M. Behrens, *Chem. – Eur. J.*, 2021, **27**, 16809–16833.
5 V. R. Choudhary, A. Dhar, P. Jana, R. Jha and B. S. Uphade, *Green Chem.*, 2005, **7**, 768–770.
6 V. R. Choudhary, R. Jha and P. Jana, *Green Chem.*, 2007, **9**, 267–272.
7 A. Abad, A. Corma and H. García, *Chem. – Eur. J.*, 2008, **14**, 212–222.
8 C. M. Crombie, R. J. Lewis, R. L. Taylor, D. J. Morgan, T. E. Davies, A. Folli, D. M. Murphy, J. K. Edwards, J. Qi, H. Jiang, C. J. Kiely, X. Liu, M. S. Skjøth-Rasmussen and G. J. Hutchings, *ACS Catal.*, 2021, **11**, 2701–2714.
9 P. Weerachawanasak, G. J. Hutchings, J. K. Edwards, S. A. Kondrat, P. J. Miedziak, P. Prasertham and J. Panpranot, *Catal. Today*, 2015, **250**, 218–225.
10 S. Meher and R. K. Rana, *Green Chem.*, 2019, **21**, 2494–2503.
11 C. H. Liu, C. Y. Lin, J. L. Chen, K. T. Lu, J. F. Lee and J. M. Chen, *J. Catal.*, 2017, **350**, 21–29.
12 F. Wang, G. Hao, Y. Guo, X. Ma and L. Yang, *Open J. Met.*, 2017, **07**, 59–68.
13 G. Wu, X. Wang, N. Guan and L. Li, *Appl. Catal., B*, 2013, **136–137**, 177–185.
14 V. Ravat, I. Nongwe and N. J. Coville, *ChemCatChem*, 2012, **4**, 1930–1934.
15 V. M. Shinde, E. Skupien and M. Makkee, *Catal. Sci. Technol.*, 2015, **5**, 4144–4153.
16 M. Gurrath, T. Kuretzky, H. P. Boehm, L. B. Okhlopkova, A. S. Lisitsyn and V. A. Likholobov, *Carbon*, 2000, **38**(8), 1241–1255.
17 C. E. Chan-Thaw, A. Savara and A. Villa, *Catalysts*, 2018, **8**, 431.
18 L. E. Betancourt, Á. M. Ortiz-Rodríguez, J. Corchado-García and C. R. Cabrera, *ACS Appl. Energy Mater.*, 2019, **2**, 287–297.
19 T. Soboleva, X. Zhao, K. Malek, Z. Xie, T. Navessin and S. Holdcroft, *ACS Appl. Mater. Interfaces*, 2010, **2**, 375–384.
20 X. Li, L. Zhao, M. Douthwaite, K. Wang, O. Akdim, I. T. Daniel, R. Oh, L. Liu, Z. Wang, F. Meng, S. Pattisson, A. López-Martin, J. Yang, X. J. Huang, R. J. Lewis and G. J. Hutchings, *ACS Catal.*, 2024, **14**, 16551–16561.
21 X. Huang, O. Akdim, M. Douthwaite, K. Wang, L. Zhao, R. J. Lewis, S. Pattisson, I. T. Daniel, P. J. Miedziak, G. Shaw, D. J. Morgan, S. M. Althahban, T. E. Davies, Q. He, F. Wang, J. Fu, D. Bethell, S. McIntosh, C. J. Kiely and G. J. Hutchings, *Nature*, 2022, **603**, 271–275.
22 I. C. Gerber and P. Serp, *Chem. Rev.*, 2020, **120**, 1250–1349.

23 B. Donoeva, N. Masoud and P. E. De Jongh, *ACS Catal.*, 2017, **7**, 4581–4591.
24 Y. C. Chiang and J. R. Ciou, *Int. J. Hydrogen Energy*, 2011, **36**, 6826–6831.
25 C. A. Wilde, Y. Ryabenkova, I. M. Firth, L. Pratt, J. Railton, M. Bravo-Sanchez, N. Sano, P. J. Cumpson, P. D. Coates, X. Liu and M. Conte, *Appl. Catal., A*, 2019, **570**, 271–282.
26 S. Pattisson, S. R. Dawson, G. Malta, N. F. Dummer, L. R. Smith, A. Lazaridou, D. J. Morgan, S. J. Freakley, S. A. Kondrat, J. J. Smit, P. Johnston and G. J. Hutchings, *ACS Catal.*, 2022, **12**, 14086–14095.
27 J. K. Edwards, J. Pritchard, M. Piccinini, G. Shaw, Q. He, A. F. Carley, C. J. Kiely and G. J. Hutchings, *J. Catal.*, 2012, **292**, 227–238.
28 U. C. Abubakar, K. R. Alhooshani, S. Adamu, J. Al Thagfi and T. A. Saleh, *J. Cleaner Prod.*, 2019, **211**, 1567–1575.
29 J. M. M. Tengco, Y. K. Lugo-José, J. R. Monnier and J. R. Regalbuto, *Catal. Today*, 2015, **246**, 9–14.
30 N. Fairley, V. Fernandez, M. Richard-Plouet, C. Guillot-Deudon, J. Walton, E. Smith, D. Flahaut, M. Greiner, M. Biesinger, S. Tougaard, D. Morgan and J. Baltrusaitis, *Appl. Surf. Sci. Adv.*, 2021, **5**, 100112.
31 C. J. Powell and A. Jablonski, *Surf. Interface Anal.*, 2000, **29**, 108–114.
32 G. Fagherazzi, P. Canton, P. Riello, N. Pernicone, F. Pinna and M. Battagliarin, *Langmuir*, 2000, **16**, 4539–4546.
33 G. Bergeret and P. Gallezot, in *Handbook of Heterogeneous Catalysis*, 2008.
34 M. H. Atwan, C. L. B. Macdonald, D. O. Northwood and E. L. Gyenge, *J. Power Sources*, 2006, **158**, 36–44.
35 S. Pérez-Rodríguez, E. Pastor and M. J. Lázaro, *Int. J. Hydrogen Energy*, 2018, **43**, 7911–7922.
36 D. O. Antonov, E. G. Silkis and B. K. Zuev, *J. Anal. Chem.*, 2021, **76**, 578–584.
37 Y. Bourlier, M. Bouttemy, O. Patard, P. Gamarra, S. Piotrowicz, J. Vigneron, R. Aubry, S. Delage and A. Etcheberry, *ECS J. Solid State Sci. Technol.*, 2018, **7**, P329–P338.
38 L. Zhang, L. Y. Tu, Y. Liang, Q. Chen, Z. S. Li, C. H. Li, Z. H. Wang and W. Li, *RSC Adv.*, 2018, **8**, 42280–42291.
39 D. J. Morgan, *C*, 2021, **7**, 51.
40 D. G. Castner, K. Hinds and D. W. Grainger, *Langmuir*, 1996, **12**, 5083–5086.
41 R. Burgess, C. Buono, P. R. Davies, R. J. Davies, T. Legge, A. Lai, R. Lewis, D. J. Morgan, N. Robinson and D. J. Willock, *J. Catal.*, 2015, **323**, 10–18.
42 S. M. S. Kumar, N. Hidyatai, J. S. Herrero, S. Irusta and K. Scott, *Int. J. Hydrogen Energy*, 2011, **36**, 5453–5465.
43 J. M. M. Tengco, Y. K. Lugo-José, J. R. Monnier and J. R. Regalbuto, *Catal. Today*, 2015, **246**, 9–14.
44 R. Banerjee and J. R. Regalbuto, *Appl. Catal., A*, 2020, **595**, 117504.
45 X. Wang, G. Wu, N. Guan and L. Li, *Appl. Catal., B*, 2012, **115–116**, 7–15.
46 Q. Lv, Q. Meng, W. Liu, N. Sun, K. Jiang, L. Ma, Z. Peng, W. Cai, C. Liu, J. Ge, L. Liu and W. Xing, *J. Phys. Chem. C*, 2018, **122**, 2081–2088.
47 M. Sankar, E. Nowicka, R. Tiruvalam, Q. He, S. H. Taylor, C. J. Kiely, D. Bethell, D. W. Knight and G. J. Hutchings, *Chem. – Eur. J.*, 2011, **17**, 6524–6532.
48 H. Wang, X. K. Gu, X. Zheng, H. Pan, J. Zhu, S. Chen, L. Cao, W. X. Li and J. Lu, *Sci. Adv.*, 2019, **5**, eaat6413.